Decaying stratified grid turbulence measurements

Adrien Thacker [1] and Olivier Eiff[1,2]

[1] Institut de Mécanique des Fluides, Université de Toulouse, CNRS-INPT-UPS,
[2] Institute for Hydrodynamics, Karlsruhe Institute of Technology,
olivier.eiff@kit.edu

Abstract

Decaying grid-generated stratified turbulence experiments were carried out in large towing tanks using 2D PIV and a newly-developed 3D-3C scanning PIV method. The creation of index-matched stable density stratifications in towing tanks up to 20 m long enabled the PIV measurements to be performed during all phases of the decay in order to attain, measure and characterize all regimes - including the elusive strongly-stratified regime (e.g. Brethouwer et al. (2007)). The complete set of turbulence statistics permitted the transitions between regimes to to be identified and defined, from quasi-isotropic to weakly-stratified, to strongly- stratified and finally to viscosity-affected, the latter being the late-time regime usually measured when localized turbulence is largely suppressed and the motion is quasi 2D.

1 Introduction

Until relatively recently, it was assumed that the vertical Froude number $F_v = U/(NL_v)$ in the limit of strong stratification at low horizontal Froude number $F_h = U/(NL_h)$ tends to zero (Riley and Lelong (2000)). The assumption implies a decoupling of horizontal layers and the turbulence can be considered quasi two-dimensional with vertical gradients. Yet, while the scaling analyses of Riley et al. (1981) and Lilly (1983) predict a vertical scale L_v much smaller than the buoyancy scale U/N, the experimental observations of Fincham et al. (1996) and Billant and Chomaz (2000) suggested that the vertical scaling of pancake structures might not imposed by initial conditions of the turbulence but instead by the flow itself. In accordance, Billant and Chomaz (2001) argued through a self-similarity analysis of inviscid flows for $F_h << 1$ that $U/N \approx L_v$, i.e. that $F_v \approx 1$ or $F_h \approx L_v/L_h (= \alpha)$ This analysis, supported by Riley and deBruynKops (2003) and Waite (2011) suggests the development of Kelvin-Helmholtz instabilities owing to a local low Richardson number (Brethouwer et al. (2007), Augier et al. (2015)) in regions of high shear between layers of pancake vortices. The development of those shear instabilities would permit a downscale energy cascade. This process is described as the "strongly stratified turbulence regime" argued to be similar to upper oceanic and the middle atmospheric turbulence (Brethouwer et al. (2007), Lindborg (2006)).

Of course in oceanic or atmospheric stratified turbulence the Reynolds number is also very large. In the laboratory or in numerical simulations, low horizontal Froude numbers come at the expense of lower Reyolds numbers. As shown by Brethouwer et al. (2007), when $Re_b = ReF_h^2 >> 1$ (Re_b is the buoyancy Reynolds number), vertical advection dominates viscous diffusion, again suggesting the scaling $U/N \approx L_v$. On the other hand, when $Re_b = ReF_h^2 << 1$, viscous diffusion dominates, implying a viscosity-affected stratified flow regime. It is the latter regime which one can surmise to have been observed in most laboratory flows such as Praud et al. (2005). Not necessarily because the strongly-stratified turbulence regime cannot be obtained, but because it cannot be measured, in

particular with standard optical methods. Indeed, if Kolmogorov-like turbulence persists in the strongly stratified regime at smaller scales, then the induced mixing of the refractive-index gradient in density stratified flows (usually via salt), will cause significant blurring and distortions, rendering measurements impossible.

2 Experimental set-up

The experiments were carried out in two differently-sized tanks at the CNRM-GAME hydraulic laboratory of Météo-France, a medium one of size $L \times H \times W = 7 \times 0.7 \times 0.8m^3$ and a large one of size $L \times H \times W = 22 \times 1 \times 3m^3$.

The turbulence was generated by towing a grid in a linearly stratified fluid at rest, with refractive-index matching. The resulting turbulence was measured via 2D and 3D-3C Scanning Particle Image Velocimetry (PIV) techniques, fixed in the laboratory frame of reference in the center of the tanks, after the passage of the grids, so that the turbulence decay could be measured in a fixed frame of reference. The grids were composed of nine sharp-edged vertical bars with a spacing of $M = 8.9$ cm for the medium tank and $M = 33$ cm for the large tank. In order not to perturb the free surface with the bars, the vertical bars did not traverse the free-surface but instead with NACA 12 profiles extending a few centimeters into the water and connected to the bars by a thin horizontal plate to reduce perturbations. Foam baffles were also installed at each end of the tanks, in order to absorb waves.

2.1 Refractive-index matching of stratification

The procedure to generate standard salt-stratified stratifications is to use one reservoir filled with water and another with a saline solution. Two computer-controlled pumps and an in-line fluid mixer are then used to uniformly inject the time-varying mixture either from the bottom (in the medium tank) or a set of floaters (in the large tank). To investigate the early and interesting phases of the decay via PIV it was necessary to effectively eliminate the refractive index (RI) variations. Daviero et al. (2001) had shown the feasibility of using ethanol alcohol in addition to salt in a medium size tank (4000 L) with density differences up to 20 kg/m^3 for the investigation of a jet in a crossflow in a linear stratification with refractive index variations less than 0.0001. In this study it is necessary to match the index of up to 60000 L over density differences over about 40 kg/m^3. Calibration curves relating the refractive index (RI) to the concentration of ethanol and salt (sea-salt) were obtained to predict the necessary concentrations and volumes in the reservoirs. Then, the ethanol, which is lighter than water, is mixed with water in the water reservoir to obtain the same RI as the saline solution in the other reservoir. The absolute density levels were chosen to both minimize the ethanol concentrations and to allow neutrally buoyant PIV seeding around the center of the stratification. Typically, the linear stratifications were made over a height of 60 cm in the medium tank and over 95 cm in the large tank, yielding buoyancy frequencies $N = \sqrt{\frac{-g}{\rho_o}\frac{d\rho}{dz}}$ of about 0.7 and 0.65 rad/s, respectively. For PIV tracers, sorted polyamide particles of about 60 μm were used in the medium tank and sorted expanded polystyrene particles of about 100 μm in the large tank.

2.2 Flow measurement configurations and parameters

The velocity fields were measured both with a 2D PIV technique and a 3D-3C Scanning PIV technique described in Albagnac et al, (2013). The 2D technique was used to measure in the central vertical plane just after the passage of the grid in the medium tank. A 12-bit X-Stream XS-1 CMOS camera with 1260 x 1024 pixel resolution acquiring images up to 200 fps was used in combination with a 25 W continuous Argon-Ion Laser to capture bursts of 12 images for three different grid towing velocities (10, 20 and 40 cm/s). Since the turbulent velocities decay very rapidly in the initial times, the multiple time-intervals in each burst allowed the PIV time-intervals to be optimized along the decay. A summary of the flow parameters for the three velocities is given in Table 2 below (Exp. M2Dx).

The 3D-3C scanning PIV technique was used in both tanks. It allows volumetric measurements of the three velocity components with subpixel resolution and therefore to also compute the velocity gradients in all directions. The technique measures truly volumetric velocity fields simultaneously, in the standard PIV sense. Pixel displacements can be extended to about 20 pixels since there is no out-of-plane particle loss. Volumetric particle images are constructed by simple superposition of the sequentially acquired and overlapping 2D images, without the need to reconstruct the particle positions as in tomographic PIV, which allows higher particle densities. Each volume is composed of several hundred overlapping images from a single high-speed camera (here between 100 and 400) rather than the usual four images from four cameras in tomographic techniques, with a consequently higher information content. The number of 2D images per volume gives the number of voxels in the scanned direction. The technique is particularly well adapted to hydraulic flows where it allows larger volumes to be measured, of particular interest here.

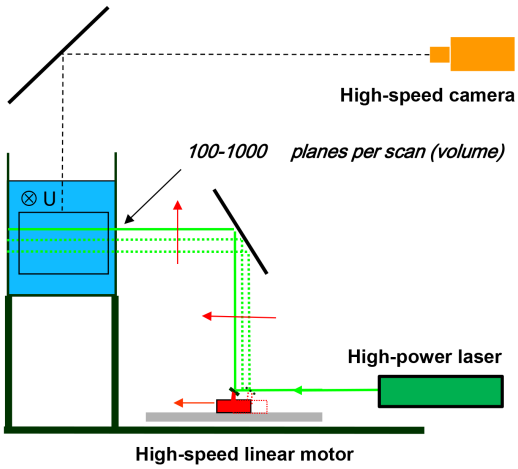

Figure 1: Sketch of 3D-3C Scanning PIV set-up. Not to scale, actual distances are much larger.

A schematic configuration for the large tank is shown in Figure 1 where the volume is scanned in the vertical direction in order to attain a horizontal extend in the 2D image plane of about 1 m or $3M$, with a height of up $1M$ in the scanning direction. In all configurations the linear motor described in Albagnac et al, (2013) was used, which attains speeds of 10 m/s and accelerations of 25 g. In the medium tank, an 8-bit 1024 x 1024 pixel Fastcam APX 3000 CMOS camera was used with up to 3000 fps at full resolution.

In the large tank, a 12-bit 1024 x 1024 pixel Photron Fastcam SA-1 CMOS camera was used with up to 5400 fps at full resolution. In the medium tank, the flow was scanned in the transverse direction to obtain a fine-scaled resolved vertical plane of $1M \times 1.2M$ over a relatively thin lateral thickness of $0.2M$. A summary of the configurations and associated flow parameters is given in Table 2 below (Exp. M3Dx in the medium tank and Exp. L3Dx in the large tank). Spacial resolutions were 2 mm for the M2Dx and M3Dx series and $15mm$ for the L3Dx series. The number of vectors in each volume was about 40000 in the M3Dx series and between 8000 and 65000 in the L3Dx series. It should be noted that resolutions were essentially limited by seeding, particularly challenging in IR matched stratifications.

Table 1: Flow parameters for the three types of experiments. M2Dx: 2D PIV in vertical plane in the medium tank; M3Dx: 3D-3C scanning PIV in the medium tank (M=8.9 cm); L3Dx: 3D-3C scanning PIV in the large tank (M=33 cm).

Exp	U_0 (cm/s)	M (cm)	N (rad/s)	Re_0	F_0	$L_x/M \times L_y/M \times L_z/M$	$Nt_i - Nt_f$
M2Da	10	8.9	0.7	8900	1.6	$1 \times (-) \times 1$	1.7-75.2
M2Db	20	8.9	0.7	17800	3.2	$1 \times (-) \times 1$	0.5-71.2
M2Dc	40	8.9	0.7	35600	6.4	$1 \times (-) \times 1$	0.4-35.7
M3Da	10	8.9	0.7	8900	1.6	$1 \times 0.2 \times 1.2$	9.1-25.9
M3Db	20	8.9	0.7	17800	3.2	$1 \times 0.2 \times 1.2$	9.1-25.9
M3Dc	40	8.9	0.7	35600	6.4	$1 \times 0.2 \times 1.2$	9.1-25.9
L3Da	5	33	0.6	16500	0.25	$2 \times 3 \times 0.2$	8-152.8
L3Db	10	33	0.6	33000	0.5	$2 \times 3 \times 0.2$	4-147.2
L3Dc	10	33	0.6	33000	0.5	$2 \times 3 \times 1$	19.8-24
L3Dd	13	33	0.6	42900	0.7	$2 \times 3 \times 1$	19.8-24
L3De	18	33	0.6	59400	0.9	$2 \times 3 \times 1$	19.8-24
L3Df	23	33	0.6	75900	1.2	$2 \times 3 \times 1$	19.8-24

Table 2: Flow parameters for the three types of experiments. M2Dx: 2D PIV in vertical plane in the medium tank; M3Dx: 3D-3C Scanning PIV in the medium tank (M=8.9 cm); L3Dx: 3D-3C Scanning PIV in the large tank (M=33 cm).

3 Results

3.1 3D fields

Figures 2(a) and (b) show the vorticity fields and streamlines issued from the 3D-3C scanning PIV technique in the large tank for Exp. L3Db (Re_0 = 33000 and F_0 = 0.5) at two different times in the decay, Nt = 107 and Nt = 24, respectively. The former at Nt= 107 clearly reveals the classical pancakes as measured via 3D-2C PIV by Praud et al. (2005) without RI matching. Smooth and rather flat structures can be identified. At Nt = 24, however, although the structures still exhibt pancake-like characteristics, strong overturning between layers is also observed. At these early times, PIV images are completely blurred without RI matching by the turbulence-induced mixing, making any optical measurements impossible.

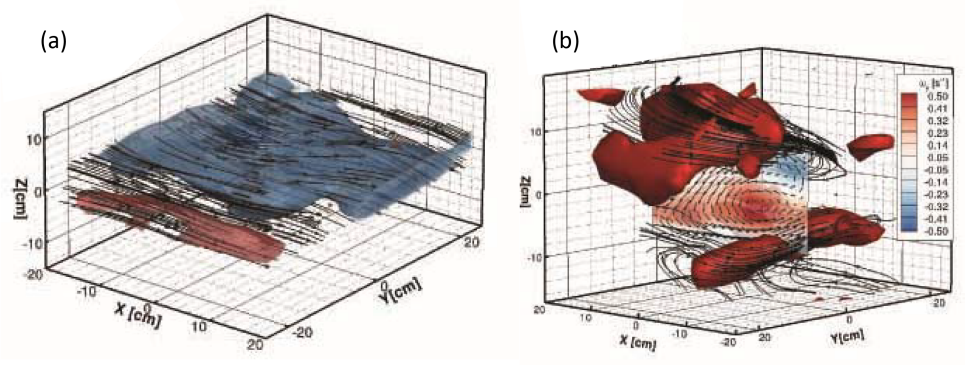

Figure 2: Vorticity fields and streamlines from 3D-3C PIV for Exp. L3Db ($Re_0 = 33000$ and $F_0 = 0.5$) at two different times in the decay: (a) Nt = 107, blue: iso-surface of $\omega_y = -0.02s^{-1}$, red: iso-surface of $\omega_y = +0,02s^{-1}$. (b) Nt = 24, red: iso-surface of $\omega_z = +0.2s^{-1}$.

3.2 Decay laws

The turbulence statistics were computed via ensemble-averaging in each measured volume. Mean velocities were first computed in each direction in order to account for slight non-zero biases due to the finite-sized sampling volumes. Velocity fluctuations and RMS values were then computed in each direction and finally averaged. Correlations and integral scales were computed accordingly with zero mean velocities. All gradient quantities such dissipation, vorticity and enstrophy were computed with 3D smoothing splines used in the PIV algorithms to replace wrong vectors and reinterpolate the irregular velocity grid onto a regular grid as in direct correlation methods of 2D PIV (see Fincham and Spedding (1997)).

Figures 3(a) and (b) show the local (turbulent) horizontal and vertical Froude numbers, $F_h = \frac{\sigma_u}{NL_h}$ and $F_v = \frac{\sigma_u}{NL_v}$, normalized by the forcing Froude number, respectively, where (σ_u, σ_v) are the longitudinal and transverse RMS velocities and (L_h, L_v) are the horizontal and vertical integral scales. A best fit of the data in the range shown reveals powerlaw decay for both normalized Froude numbers with the same exponent, t^{-1}. This implies that both normalized Froude numbers decay as Nt^{-1}, albeit with different proportionality coefficients, and are therefore independent of the forcing parameters Re_o and F_o. Furthermore, it can be shown that the measured power law decay exponents of L_h ($\propto t^{0.2}$) and σ_u ($\propto t^{-0.8}$) are consistent with Taylor's estimate $L_h \propto \sigma_u^3/\epsilon$ and the dissipation rate given by $\epsilon \propto -d\sigma_u^2/dt$.

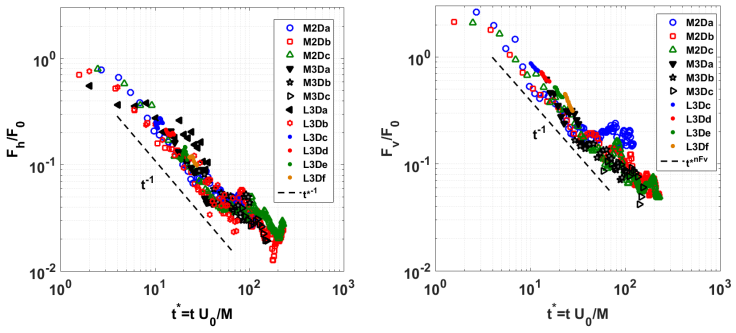

Figure 3: Decay of turbulent Froude numbers: (a) horizontal F_h and (b) vertical F_v.

3.3 Regime transitions

Figure 4 shows the ratio of the longitudinal to the vertical RMS velocities, $\gamma_{u-w} = \sigma_u/\sigma_w$, as a function of the turbulent horizontal Froude number. It can be observed that for initial times when $F_h > 1$, this anisotropy ratio is of order one, i.e., the turbulence is close to being isotropic. However, when F_h drops below one, the ratio increases strongly. As expected, for low F_h, stratification suppresses the vertical motions. It can be shown that this occurs at critical time $Ntc_1 = C_{F_h} = 2.7$ - independently of R_0 and F_0, where C_{F_h} is the measured proportionality coefficient of the horizontal Frounde number decay law. This is consistent with the observed "collapse" time of turbulent wakes $Nt \simeq 2$ (Bonnier and Eiff (2002). According the proposed regime diagram of Brethouwer et al. (2007), after this transition one can expect to be in the weakly stratified regime.

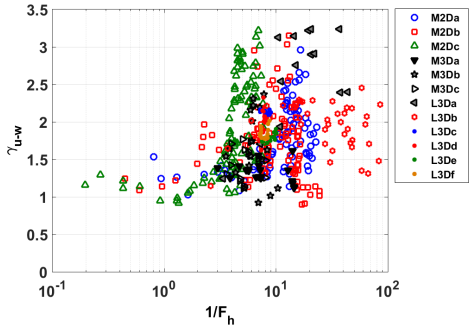

Figure 4: Anistropy ratio σ_u/σ_w as a function of the horizontal turbulent Froude number F_h. The decay time is from left to right.

To show that the strongly-stratified regime is subsequently attained, Figure 5 shows the dependence of the aspect ratio of the vertical integral scale to the horizontal integral length scale $\alpha = L_v/L_h$ as a function of F_h (Figure 5a) and F_v (Figure 5b). In both figures the Froude number is increasing from left to right, implying that the flow evolution should be read from right to left. It can be seen in Figure 5a that α drops of from about 0.35 at F_h around 0.2 with a slope of $F_h = 3\alpha$. This implies a constant vertical Froude number of 1/3, as seen in Figure 5b, in good agreement with the self-similarity analysis $F_v \simeq 1$ scaling proposed by Billant and Chomaz (2001), concurring that the strongly stratified regime has been attained. The 3D view seen earlier in Figure 2(b) pertains to this regime, with strong K-H overturns. The transition from weakly to strongly-stratified turbulence is again independent of the forcing parameters, occurring at $Nt \approx 19$.

Figure 6 shows the evolution of total dissipation ϵ and its decomposition into horizontal and vertical components, ϵ_h and ϵ_v. Here, a 3D experiment in the medium tank is shown which better resolves the small scales. It can be shown that while ϵ_v also decays, it decays slower than the total dissipation ϵ, therefore approaching it. This is in accordance with the dissipation being dominated by the vertical shearing of the pancake-like vortices in the viscosity-affected regime as seen in Figure 2(a). The approach of ϵ_v levels off at $\epsilon_v/\epsilon \approx 80\%$ which occurs at around $R_b \approx 1$, in accordance with the transition to the viscosity-affected regime in the regime diagram of Brethouwer et al. (2007). It should be noted though the critical time to this transition is dependent on the forcing parameters. If this critical time is below the critical time to achieve the strongly stratified regime, the strongly stratified regime is bypassed.

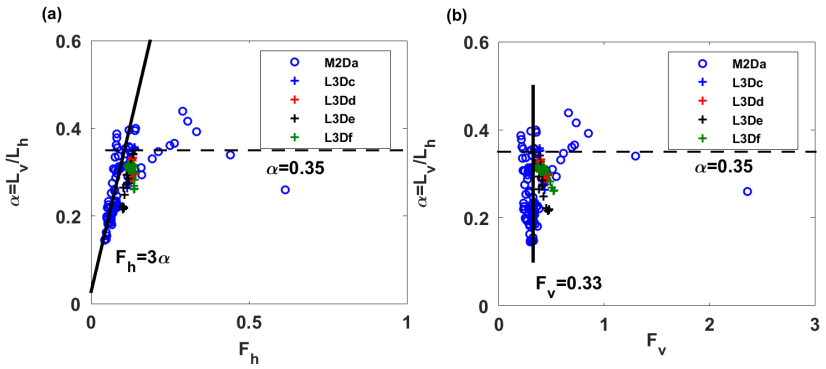

Figure 5: Length-scale aspect ratio $\alpha = L_v/L_h$ as a function of (a) F_h and (b) F_v.

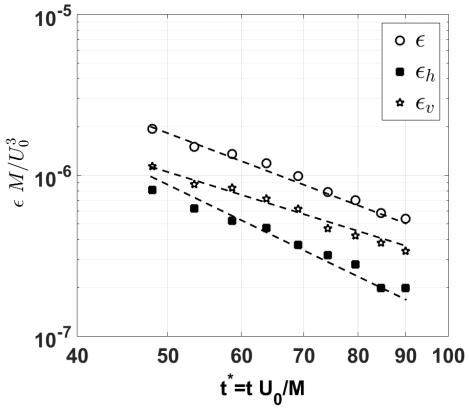

Figure 6: Total dissipation ϵ and its horizontal ϵ_h and vertical ϵ_v components. Data for Exp. M3Dc.

4 Conclusion

The decaying grid turbulence in refractive-index matched stable stratifications was measured from the initial quasi-isotropic regime before the turbulence collapses till the well-known viscosity-affected regime. Statistical analysis of the velocity data obtained via 2D and 3D PIV suggests that the strongly-stratified regime at low horizontal Froude number has been attained, marked by a buoyancy Reynolds number greater than one and a vertical Froude number based on a vertical integral scale of order one, confirming the new scaling view of stratified turbulence of Billant and Chomaz (2001) and the numerical simulations of Brethouwer et al. (2007).

Acknowledgments The authors would like to thank numerous colleagues of Météo-France and IMFT as well as several students who have helped to realize the experiments and measurements: S. Benzennou, N. Boulanger, J.-C. Boulay, J.-C. Canonici, S. Cazin, E. Cid, J. Favier, C. Merlo, F. Moulin & A. Paci. We would also like to thank A. Fincham and J. Riley for helping to conceive the first experiments and A. Fincham in the development of the 3D-3C scanning PIV technique. The work was financially supported by the Fondation STAE (ITAAC project).

References

J. Albagnac, F.Y. Moulin, O. Eiff, L. Lacaze, P. Brancher, "A three-dimensional experimental investigation of the structure of the spanwise vortex generated by a shallow vortex dipole", Environ Fluid Mech. **14**:957–970 (2013).

P. Augier, P. Billant and J.-M. Chomaz, "Stratified turbulence forced with columnar dipoles: numerical study". J. Fluid Mech. **769**, 403-443 (2015).

P. Billant and J.M. Chomaz, "Experimental evidence for a new instability of a vertical columnar vortex pair in a strongly stratified fluid", J. Fluid Mech. **418**, 167-188 (2000).

P. Billant and J.-M. Chomaz, "Self-similarity of strongly stratified inviscid flows", Phys. Fluids **13**, 1645 (2001).

M. Bonnier and O. Eiff, "Experimental investigation of the collapse of a turbulent wake in a stably stratified fluid", Phys. Fluids **14**, 791 (2002).

G. Brethouwer, P. Billant, E. Lindborg and J.-M Chomaz, "Scaling analysis and simulation of strongly stratified turbulent flows", J. Fluid Mech. **585**, 343 (2007).

G.J. Daviero, P.J.W. Roberts, K. Maile, "Refractive index matching in large-scale stratified experiments", Exp. Fluids, **31**, 119-126 (2001).

A.M Fincham, T. Maxworthy and G.R. Spedding, "Energy dissipation and vortex structure in freely decaying, stratified grid turbulence", Dyn. Atmos. Oceans **19**, 155 (1996).

A. M. Fincham, G. R. Spedding, "Low cost, high resolution DPIV for measurement of turbulent fluid flow", Exp. Fluids **23**, 449-462 (1997).

D.K. Lilly, "Stratified turbulence and the mesoscale variability of the atmosphere", J. Atmos. Sci.**40**, 749 (1983).

E. Lindborg, "The energy cascade in a strongly stratified fluid", J. Fluid Mech. **550**, 207 (2006).

O. Praud, A.M. Fincham, and J. Sommeria, "Decaying grid turbulence in a strongly stratified fluid", J. Fluid Mech. **522**, 1 (2005).

J.J. Riley, R.W. Metcalfe and M.A. Weissman, "Direct numerical simulations of homogenous turbulence in density-stratified fluids", AIP Conference Proceedings **76**, 79 (1981).

J.J. Riley and M.-P. Lelong, "Fluid motions in the presence of strong stable stratification", Annu. Rev. Fluid Mech. **32**, 613, (2000).

J.J. Riley and S.M. deBruynKops, "Dynamics of turbulence strongly influenced by buoyancy", Phys. Fluids **15**, 2047 (2003).

M.L. Waite, "Stratified turbulence at the buoyancy scale", Phys. Fluids **23**, 066602 (2011).